ISSN 0016-7029, Geochemistry International, 2021, Vol. 59, No. 2, pp. 156–170. © Pleiades Publishing, Ltd., 2021.
Russian Text © The Author(s), 2021, published in Geokhimiya, 2021, Vol. 66, No. 2, pp. 145–160.

Oxygen Isotope Composition in Olivine and Melts from Cumulates of the Yoko-Dovyren Layered Massif, Northern Transbaikalia, Russia

A. A. Ariskin[a, b, *], I. S. Fomin[c], E. O. Dubinina[d], A. S. Avdeenko[d], and G. S. Nikolaev[b]

[a] *Geological Faculty, Moscow State University, Leninskie gory, Moscow, 119234 Russia*

[b] *Vernadsky Institute of Geochemistry and Analytical Chemistry (GEOKhI), Russian Academy of Sciences, Moscow, 119991 Russia*

[c] *Department of Earth and Environmental Sciences Level 1, 12 Wally's Walk Macquarie University, NSW 2109, Australia*

[d] *Institute of Geology of Ore Deposits, Petrography, Mineralogy and Geochemistry, Russian Academy of Sciences, Moscow 119017, Russia*

**e-mail: ariskin@rambler.ru*

Received March 22, 2020; revised June 7, 2020; accepted June 7, 2020

Abstract—Oxygen isotope composition was studied in 33 monomineralic fractions of olivine from plagioclase lherzolite, dunite, troctolite, and olivine gabbronorite of the Yoko-Dovyren layered massif. The $\delta^{18}O$ values of the least altered rocks not contaminated with crustal materials range within 5.8 ± 0.2‰ ($n = 27$). These values for the dunite contaminated with carbonate material are notably higher and average at 6.2 ± 0.3‰. This is similar to characteristics of the Bushveld and Jinchuan mineralized complexes. Using the COMAGMAT-5 model, the temperatures of equilibrium of 98% crystals with late portions of the residual melts were evaluated at 1131–1266°C (1176 ± 34°C on average). These estimates are viewed as the closing temperatures of the cumulate systems with respect to the efficient exchange of ^{18}O and ^{16}O isotopes between olivine and mobile melt/fluid. For the uncontaminated systems, the $\delta^{18}O$ values of the parental melt calculated using the modeled temperatures are 6.6 ± 0.2‰, and are 7.1 ± 0.3 ‰ for melts with signatures of crustal contamination. Such relations are consistent with insignificant (no more than a few percent) contamination of the parental magmas with carbonate materials from the host rocks.

Keywords: oxygen isotope composition, olivine, layered intrusion, COMAGMAT, efficiency of contamination

DOI: 10.1134/S0016702921020026

INTRODUCTION

The Yoko-Dovyren layered massif is located 60 km north of the northern tip of Baikal Lake and belongs to the Dovyren intrusive complex, which is dated at ~728 Ma (Ariskin et al., 2013; Ernst et al., 2016). The massif is clearly discernible in the local topography: it composes a range up to 2114 m high, which extends northeastward for approximately 26 km and is cut by the valley of the Ondoko River, thus being divided into two mounts: Yoko and Dovyren (Gurulev, 1965; Konnikov, 1968). The nearly vertical dips of the rocks, which is conformable with the dips of the host carbonate–terrigenous rocks of the Middle–Late Riphean Olokit complex (Rytsk et al., 2002) allowed for a detailed mapping of the modal and compositional layering (Kislov, 1998; Ariskin et al., 2018a). In its thickest (up to 3.4 km) central part, the rock sequence of this massif consists of a basal horizon of plagioperidotites, which gives way upward to plagioclase and adcumulus dunites, with a sharp transition to troctolites (varying from melano- to leucocratic lithologies), and the vertical section is crowned by gabbroids, which vary from leucotroctolites and olivine gabbro to olivine and olivine-free gabbronorites and (at the roof) to pigeonite-bearing gabbro. Dunites are practically absent from the northeastern and southwestern closures of the intrusion, and these portions of the massif are dominated by melanotroctolites and leucogabbroids (NE, Shkolnyi section). Mount Yoko is made up of interbedding troctolites and olivine gabbro (Fig. 1). The basal horizons in the margins are similar in structure: in both of them, the rocks composing the very bottom of the sequence are plagioperidotites, which are a little bit less primitive that in the core of the intrusion. Correspondingly, pigeonite-bearing gabbro are more widely spread near the top portion of the massif.

The reasons for long-lasting interest in this massif are as follows. First of all, this is because the Dovyren intrusive complex is accompanied by Cu–Ni sulfide ores, which were found in underlying sills and tongues of the main body (Gurulev, 1965; Konnikov, 1986). Also, domains with low-sulfide PGE mineralization were found in the leucotroctolites and anorthosites and are referred to as Reef I (Distler and Stepin, 1992; Orsoev et al., 1995; Konnikov et al., 2000) or the Main

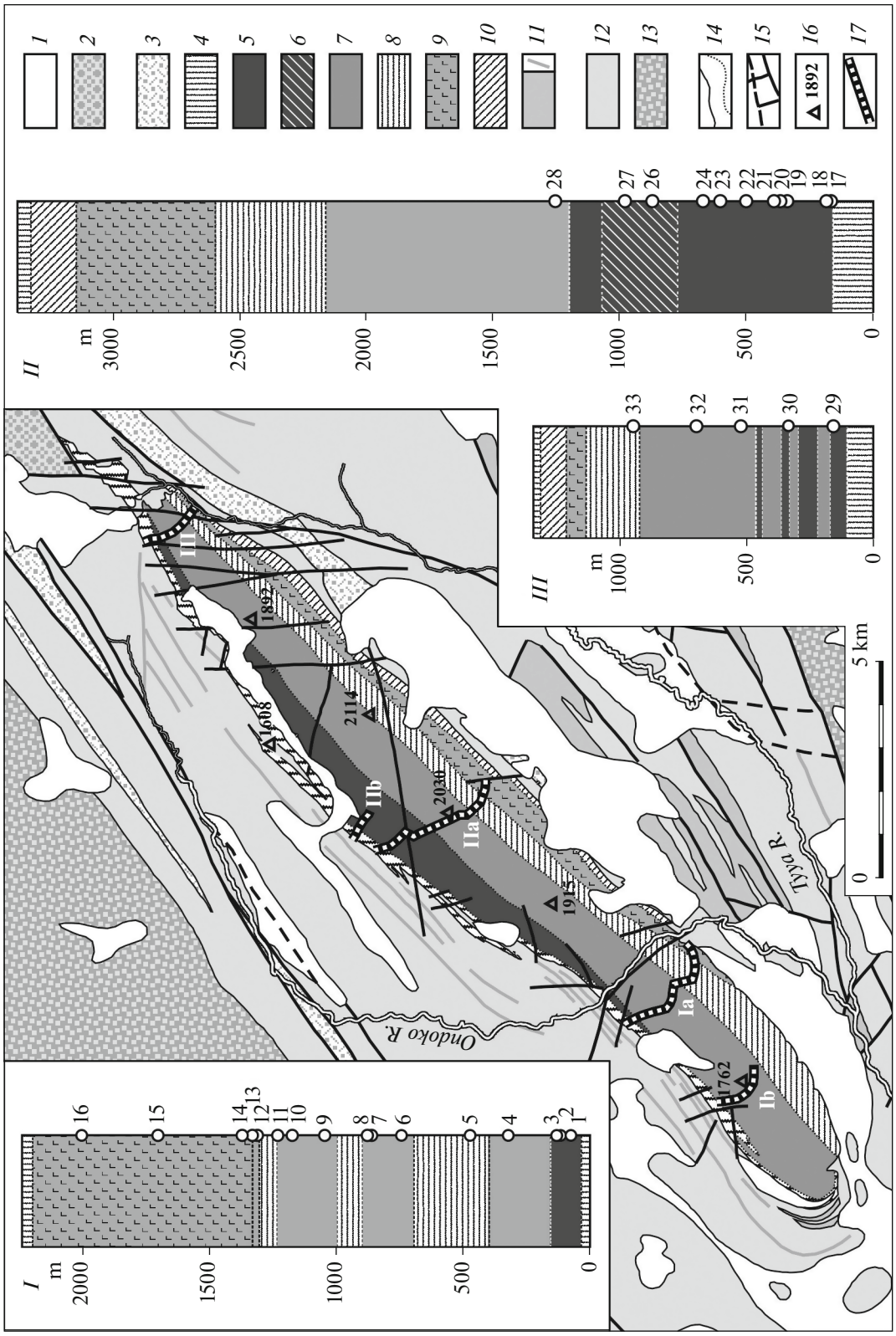

Fig. 1. Schematic geological map of the Yoko-Dovyren massif [based on geological maps by A.G Krapivin (Bushuev and Tarasova, 1985) and A.G. Stepina (Stepin and Vlasenko, 1994)]. Insets show summarizing vertical sections and a schematic location map of the sampling sites). (*I*) Southwestern part of the massif (Yoko vertical section), (*II*) central part (near Bolshoi and Tsentralnyi streams), (*III*) northeastern termination of the massif (vertical section in the Shkolnyi area). Legend: (*1*) Quaternary rocks (Q_{II-IV}); (*2*) Kholodninskaya Formation ($V-\in_1$); (*3–11*) Synnyr–Dovyren volcanic–plutonic complex (R_{2-3}): (*3*) Inyaptuk Formation, (*4–11*) Dovyren intrusive complex: (*4*) Marginal Group: picrodolerites, diabases, and plagioclase lherzolites near the bottom of the massif and ophitic diabases in the near-roof part, (*5*) dunites, (*6*) contaminated dunites, (*7*) troctolites, (*8*) olivine gabbro, (*9*) olivine gabbronorites and norites, (*10*) quartz–pigeonite gabbronorites; (*11*) not subdivided; (*12*) carbonate–terrigenous rocks of the Synnyr rift (R_{2-3}); (*13*) terrigenous and carbonate–terrigenous rocks of the Olokit trough (R_{2-3}); (*14*) geological boundaries; (*15*) faults; (*16*) elevations (Mt. Yoko 1762 m, Mt. New Dovyren 2030 m, and Mt. Dovyren 2114 m). (*17*) transects: *Ia* ans *Ib* are Yoko, *IIa* ans *IIb* are Tsentralnyi, and *III* is Shkolnyi.

Reef (Ariskin et al., 2016, 2020). These facts and age correlations of the rocks provided grounds to attribute the Dovyren massif to the eastern branch of the Late Riphean Cu–Ni–PGE East Siberian metallogenic province (Polyakov et al., 2013).

Another reason for the aforementioned interest in this massif is that it shows a set of typomorphic features that indicate that the Dovyren magma chamber was open during the early and intermediate evolution of the massif (Ariskin et al., 2018a). This follows from the dominance of ultradepleted rocks and from the evaluated (for individual geological sections) weighted mean concentrations of incompatible elements, which are three to five times higher than in the inner-contact rocks. Neither volcanics nor sills with such geochemical characteristics have ever been found in the northern West Baikal area, and this leads to the conclusion that the Dovyren rock sequence is a sort of a "residue sequence", which is made up of the crystalline residues of olivine and olivine–plagioclase cumulates that have lost up to 60–70% gabbronorite melts. In view of this, information on the composition of the parental, most primitive magmas is recorded not in the average composition of the intrusion in its various vertical sections but in the picrodolerites from its lower contact zones.

The third reason is the anomalous isotope characteristics of rocks of the Dovyren intrusive complex. Data on the Rb–Sr and Sm–Nd isotope systems of ultramafic sills underlying the Dovyren massif and the chilled gabbronorites, picrodolerites, dunites, troctolites, and gabbroids of the layered complex show that three-fourths of the rock samples define a stable cluster of compositions with extremely enriched $^{87}Sr/^{86}Sr(t)$ ratios (0.7094–0.7149 at t = 728.4 Ma) and low $\varepsilon_{Nd}(t) = -16.1$ to -13.2 (Ariskin et al., 2015). The most strongly altered, mostly serpentinized rocks lie outside this range. These facts lend support for the hypothesis that the Dovyren magmas were derived from an isotopically anomalous source (Amelin et al., 1996) and led to the conclusion that its protolith in the Neoproterozoic sublithospheric mantle may have been products of partial melting and/or metasomatic transformations of the Archean mantle at ~2.7–2.8 Ga (Ariskin et al., 2018a). It is still uncertain whether the protolith was a heterogeneous mixture of in-situ crystallized partial melts and mantle residues in supersubduction (?) mantle or it was produced by the contamination of primary mantle melts with Archean crustal material. An extrapolation of $\varepsilon_{Nd}(t)$ values for rocks of the Dovyren complex to the intersection with the mantle evolution trend in the approximation of the primary ratio Sm/Nd = 0.350 suggests that the Sm/Nd ratio of the source was close to 0.221 (Ariskin et al., 2015), which is close to the average composition of the continental crust (Taylor and McLennan, 1985). This is a serious argument in favor of the involvement of continental crustal material in forming the mantle source of the Dovyren magmas.

The Dovyren intrusive complex thus offers a unique example of distinct open-type magma chamber, whose evolution resulted in a large layered intrusion and differentiated rocks with Cu–Ni–PGE mineralization. The source of this magmatic material in the Neoproterozoic was the sublithospheric mantle, whose isotope composition (Sm–Nd system) carries information on a much older (perhaps, Neoarchean) protolith. The contrasting superposition of the problems of evolution of the magma chambers and the processes of chamber differentiation and the origin of the sublithospheric source are in the mainstream of fundamental problems of modern petrology and the theory of processes forming Cu–Ni–PGE sulfide mineralization. A solution of these problem requires further studies of the composition of the Dovyren rocks, including their stable-isotope composition, first of all, the sulfur and oxygen isotope composition. The need to update the data on the isotope composition of these elements on the basis of a larger set of rock compositions was partly dictated by progress in modern techniques of isotope analysis and the improvement of their sensitivity. The petrological–geochemical aspect is related to difficulties in distinguishing between the effects of the early crustal contamination during the origin of the mantle source and the Late Riphean assimilation of the wall rocks, a fairly probable process during magma emplacement and the development of the chamber. This problem is made even more pressing by the fact that the Dovyren intrusion hosts xenoliths of skarns that replaced carbonate rocks and contains relicts of the host rocks (Pertsev and Shabynin, 1979; Pertsev et al., 2003). The solution of the problems formulated above is even further complicated by hydrothermal–metasomatic processes, which modified large volumes of the ultramafics and gabbroids approximately 70 Ma after the solidification of the intrusion (Ariskin et al., 2013), perhaps, simultaneously with multistage epigenetic low-grade burial metamorphism (Spiridonov et al., 2019). This paper presents high-precision data on the oxygen isotope composition of olivine grains from cumulates, which were sampled along three transects across the central part of the Yoko-Dovyren massifs and its southwestern and northeastern closures.

EARLIER STUDIES

The first estimates of the oxygen isotopes in olivine were obtained in (Ustinov et al., 1980) for monomineralic fractions from dunites, troctolites, olivine gabbro, and gabbronorites from the central portion of the intrusion. Oxygen was extracted at interaction of the samples with BrF_5 or ClF_5 (Taylor and Epstein, 1962; Clayton and Mayeda, 1963), including a number of experiments on faster fluorination in autoclave reactors. The isotope ratios were measured on a MI-1201 mass spectrometer, the reproducibility of $\delta^{18}O$ values was approximately ±0.2‰. The olivine had $\delta^{18}O$

within the range of 8.1–9.2‰. With regard to additional data on the plagioclase and pyroxene, these authors have calculated the oxygen isotope composition of the original Dovyren magma ($\delta^{18}O$ = 8.5–8.7‰), i.e., notably higher values than estimates for primitive mantle magmas (Taylor, 1980), including MORB ($\delta^{18}O = 5.7 \pm 0.2$‰; Ito et al., 1987). The high $\delta^{18}O$ values have not been confirmed later, and later measurements (at the same laboratory) of olivine from picrodolerite from the lower contact zone of the massif yielded much weaker enrichment in the heavy oxygen isotope: $\delta^{18}O = 6.4$‰ (Krivoplyasov et al., 1984).

No less contradictory data were presented in (Goncharenko et al., 1992). These data were acquired by means of volumetric fluorination and subsequent analysis on a MI-1309 spectrometer (the declared reproducibility was 0.3–0.5‰). The oxygen isotope composition was measured in olivine monomineralic fractions from fifteen samples taken in the central part of the intrusion: one plagiolherzolite sample, four dunite samples, five troctolite samples, one olivine gabbronorite sample, and four olivine gabbro samples. Although the authors claimed that "the least altered rocks were used", whose LOI were lower than 2.5 wt %, the results showed widely scattered $\delta^{18}O$ values of 0.6 to 6.4‰, which were lower than the earlier measurements. Therewith two types of olivine compositions were identified: one with a mode at $\delta^{18}O = 5.5 \pm 0.7$‰ (two olivine gabbro samples, two melanotroctolites, and one olivine gabbronorite) and $\delta^{18}O = 3.0 \pm 1.1$‰ (the other ten samples, including all dunites and one plagiolherzolite from the basal zone). Based on these data, it was hypothesized that the Dovyren chamber was formed when magma with mantle signatures of oxygen isotope composition was emplaced, whereas the shift toward low $\delta^{18}O$ values correlated with traces of plastic deformations in the olivine grains. This fact was regarded as an argument that oxygen isotopes were redistributed at the syntectonic recrystallization of the rocks, perhaps, with the involvement of fluids with $\delta^{18}O$ values (Goncharenko et al., 1992).

It should be mentioned that data on the oxygen isotope composition of olivine and other refractory minerals obtained by volumetric fluorination (particularly with the application of faster decomposition of the minerals, e.g., Ustinov et al., 1980) may have introduced uncertainties related to that the minerals were not completely decomposed at external heating. As a result, the modern literature conventionally operates with data acquired either with laser heating (mostly in publications after 1995) or with SIMS.

Data on the isotope composition of 17 monomineralic fractions (olivine, plagioclase, clinopyroxene, and orthopyroxene) and eight samples from the so-called *Critical Zone* of the Dovyren massif were presented in (Orsoev et al., 2010). The Critical Zone is a unit of varying mineral composition and thickness (about 200 m on average) in the transition zone from the troctolites to olivine gabbro. The top part of the Critical Zone is made up of complicatedly interbedding meso- and leucotroctolites, leucogabbro, and related gabbro-pegmatites, which are complicated by anorthosite schlieren with disseminated low-sulfide but locally abundant PGE mineralization (Orsoev, 2019). For the first time for the Dovyren massif, the isotope composition of minerals was measured using heating with a Nd–YAG laser. The data were calibrated on the NBS-28 and NBS-30 internationally certified standards. The five $\delta^{18}O$ values obtained for the olivine varied from 4.80 to 5.8‰ (at an average of 5.1 ± 0.4‰). With regard to data on the other rock-forming minerals, the values for the rocks lied within the range of $\delta^{18}O$ = 5.4–6.1‰ (5.8 ± 0.3‰ on average, except the gabbro-pegmatite). The relatively low $\delta^{18}O$ values and the absence of oxygen isotope equilibrium with other phases were interpreted by the authors as resulting from interaction between the rocks and meteoric waters.

MATERIALS AND ANALYTICAL TECHNIQUES

Samples for the isotope study were selected with the aim of solving two problems: determine the variations in the $\delta^{18}O$ values of the olivine along the strike of the massif and across it, following the complete stratigraphic cross-section. Considering the distribution of the least altered rocks, five samples were collected in the northeastern termination of the massif, in the Shkolnyi section, which spans a range of stratigraphic levels of approximately 800 m, i.e., more than a half of the vertical section of this part of the intrusion (Table 1). In the central part of the Dovyren massif (its generalized vertical section along the Bolshoi and Tsentralnyi transects; Ariskin et al., 2018a), twelve samples were taken, which represent more than 1000 m of the vertical section of the massif (one-third of its total thickness) up from its lower contact. In the southwestern part (Yoko section), sixteen samples were collected, which represent the practically whole stratigraphic sequence. One half of the studied rocks are ultramafics (plagiolherzolites, plagiodunites, and dunites), which are contaminated in the central part because of reactions of carbonate in host-rock xenoliths with the ultramafic magma (Wenzel et al., 2002). The other half is troctolites (varying from melano- to leucocratic) and olivine gabbro (Table 1). The losses on ignition for the whole set were 0.6 ± 1.2 wt % or, with a correction for the excess mass at the complete Fe oxidation to Fe_2O_3, 1.8 ± 1.3 wt % (Table 2)[1]. For

[1] The LOI values were corrected by the formula (Lechler and Desilets, 1987) LOI* = LOI (original) + 0.11FeO, where the original value corresponds to the analytical values, and FeO is the total Fe concentration in the rock. It is therewith assumed that the oxidized Fe fraction in cumulates (particularly in an adcumulus rock) is low, and Fe^{2+} is completely oxidized in the process of annealing.

Table 1. Samples in which the oxygen isotope composition of olivine was studied

Sample	Sample number	*h*, m*	Rock	Genetic interpretation**
Yoko section, SW termination of the Yoko-Dovyren massif (thickness ~2200 m)				
1	07DV340-1	73	Mineralized plagiodunite	Olivine mesocumulate with sulfides
2	07DV232-1	~113	Plagiodunite	Olivine mesocumulate***
3	07DV231-1	130	Plagiodunite	Olivine mesocumulate***
4	07DV341-1	~320	Troctolite	*Ol*–*Pl* adcumulate
5	07DV341-3	470	Olivine gabbro	Same
6	07DV343-1	743	Olivine gabbro	"
7	07DV344-1	860	*Cpx*-bearing troctolite	"
8	07DV223-1	~878	Troctolite	"
9	07DV224-1	1045	*Cpx*- and *Pl*-bearing dunite	*Ol* cumulate in cotectic (*Ol*+*Pl*) melt
10	07DV226-1	1172	Troctolite	*Ol*–*Pl* adcumulate
11	07DV346-1	~1230	*Cpx*- and *Pl*-bearing dunite	*Ol* cumulate in cotectic (*Ol*+*Pl*) melt
12	07DV346-5	1310	Olivine gabbro	*Ol*–*Pl* adcumulate
13	07DV346-6	1330	Troctolite	Same
14	07DV346-8	1370	Olivine gabbro	"
15	07DV228-1	~1703	Olivine gabbro	"
16	07DV229-1	2005	Leucotroctolite	"
Summarizing vertical section based on outcrops along Bolshoi and Tsentralnyi streams in the central part of the massif (thickness 3380 m)				
17	07DV124-2	162	Plagiodunite	Olivine mesocumulate
18	07DV124-3	181	Plagiodunite	Olivine mesocumulate
19	07DV124-11	335	Dunite-1	Olivine adcumulate
20	07DV124-12	361	Dunite-1	Same
21	07DV124-13	387	Dunite-1	"
22	**07DV124-17**	**496**	**Dunite-2**	"
23	**07DV124-20**	**600**	**Dunite-2**	"
24	**07DV124-22**	**669**	**Dunite-2**	"
25	**07DV309-1**	**–**	**Dunite-3**	"
26	**07DV131-10**	**868**	**Dunite-3**	"
27	**07DV311-1**	**974**	**Dunite-3**	"
28	07DV314-2	1251	Troctolite	*Ol*–*Pl* adcumulate
Shkolnyi section in the NE closure of the massif (thickness 1345 m)				
29	S08-4	156	Plagiodunite	Olivine mesocumulate
30	S10-7	334	Plagiodunite/Melanotroctolite	*Ol* cumulate in cotectic (*Ol*+*Pl*) melt
31	S12-2	521	*Phl*-bearing plagiolherzolite	Olivine orthocumulate in near-cotectic magma; perhaps, an additional injection
32	S30-3	694	Melanotroctolite	*Ol* cumulate in cotectic (*Ol*+*Pl*) melt
33	S36-1	945	*Cpx*-bearing leucotroctolite	*Ol* cumulate in cotectic (*Ol*+*Pl*) melt

* Height up the vertical section from the lower contact (in m), ** Based on structural characteristics in combination with numerical simulations (with the COMAGMAT-5 software; Ariskin et al., 2018b) of the stability of the primary phases. Three dunite varieties: (*1*) hypidiomorphic-granular rocks, (*2*) rocks with a panidiomorphic-granular texture, weakly contaminated when the ultramafic magma interacted with carbonates (as follows from mineralogical features) (Wenzel et al., 2002); (*3*) strongly contaminated dunites, usually serpentinized. Below, six samples (22–27) are regarded as "contaminated" (printed in semibold type in Tables 2 and 3).

Table 2. Petrochemical and mineralogical features and $\delta^{18}O$ of olivine of rocks from the Yoko-Dovyren massif

Sample	Sample number	LOI, wt %		*Ol* (CIPW, wt %)	*Fo* (*Ol*, mol %)	CaO (*Ol*, wt %)	$\delta^{18}O$ (*Ol*, ‰)	100Cr/(Cr+Al) in spinel
		analysis	correction					
1	07DV340-1	0.17	1.90	70.1	82.4 ± 0.7	0.05 ± 0.01	6.14	69.6 ± 7.8
2	07DV232-1	–0.41	0.90	78.3	85.1 ± 0.1	0.06 ± 0.02	5.97	70.8 ± 2.6
3	07DV231-1	0.37	1.69	81.5	85.4 ± 0.2	0.06 ± 0.03	5.88	62.2 ± 4.0
4	07DV341-1	–0.71	0.64	75.2	83.2 ± 0.1	0.07 ± 0.02	5.91	69.7 ± 2.3
5	07DV341-3	0.05	0.61	16.6	80.3 ± 0.2	0.03 ± 0.01	5.79	63.7
6	07DV343-1	–0.43	0.58	46.5	80.8 ± 0.4	0.03 ± 0.01	5.70	68.8 ± 0.9
7	07DV344-1	–0.12	0.68	36.8	80.8 ± 0.2	0.04 ± 0.03	5.76	81.3
8	07DV223-1	0.13	1.31	64.5	83.0 ± 0.2	0.04 ± 0.02	5.78	68.3 ± 2.3
9	07DV224-1	–0.41	1.13	89.0	83.9 ± 0.1	0.05 ± 0.03	6.00	67.5 ± 0.8
10	07DV226-1	–0.29	0.67	51.7	82.5 ± 0.1	0.04 ± 0.02	5.80	69.6 ± 5.2
11	07DV346-1	–0.32	1.27	92.0	83.9 ± 0.1	0.11 ± 0.03	5.84	68.7 ± 1.5
12	07DV346-5	0.18	0.99	38.0	81.8 ± 0.1	0.04 ± 0.01	5.74	–
13	07DV346-6	0.27	1.06	41.9	82.7 ± 0.1	0.05 ± 0.01	5.88	72.3 ± 2.6
14	07DV346-8	0.03	0.74	18.5	77.4 ± 0.1	0.04 ± 0.01	5.66	–
15	07DV228-1	0.06	0.88	29.1	78.0 ± 0.2	0.03 ± 0.01	5.78	–
16	07DV229-1	1.32	1.95	22.1	77.6 ± 0.4	0.06 ± 0.01	5.86	69.5 ± 3.5
17	07DV124-2	0.52	1.72	73.4	86.3 ± 0.2	0.06 ± 0.02	5.32	63.8 ± 3.0
18	07DV124-3	–0.67	0.69	79.3	84.5 ± 0.1	0.04 ± 0.01	5.70	63.6 ± 3.7
19	07DV124-11	2.17	3.62	93.2	85.9 ± 0.2	0.06 ± 0.02	5.75	63.5 ± 3.6
20	07DV124-12	–0.36	0.95	88.6	86.9 ± 0.1	0.04 ± 0.01	5.99	65.2 ± 2.9
21	07DV124-13	0.69	2.12	92.0	85.7 ± 0.1	0.06 ± 0.02	5.41	63.3 ± 2.1
22	**07DV124-17**	**–0.51**	**0.74**	**96.4**	**88.1 ± 0.1**	**0.10 ± 0.02**	**6.15**	**62.6 ± 1.3**
23	**07DV124-20**	**2.11**	**3.55**	**94.2**	**85.8 ± 0.1**	**0.07 ± 0.01**	**6.01**	**62.2 ± 2.1**
24	**07DV124-22**	**3.63**	**4.99**	**96.3**	**87.6 ± 0.1**	**0.10 ± 0.02**	**5.96**	**57.9 ± 7.0**
25	**07DV309-1**	**–0.53**	**0.78**	**92.2**	**87.0 ± 0.1**	**0.19 ± 0.05**	**6.26**	**47.7**
26	**07DV131-10**	**3.76**	**5.12**	**95.2**	**87.1 ± 0.1**	**0.28 ± 0.06**	**6.95**	**40.3 ± 3.1**
27	**07DV311-1**	**3.34**	**4.68**	**90.7**	**88.4 ± 0.2**	**1.17 ± 0.01**	**6.37**	**24.4 ± 3.8**
28	07DV314-2	–0.35	0.93	74.1	82.0 ± 0.2	0.04 ± 0.04	5.75	71.3 ± 2.7
29	S08-4	0.76	2.12	75.0	83.5 ± 0.1	0.05 ± 0.01	6.37	62.3 ± 4.3
30	S10-7	0.46	2.06	86.1	83.3 ± 0.2	0.04 ± 0.01	5.60	71.5 ± 2.2
31	S12-2	1.76	2.87	65.7	86.0 ± 0.3	0.04 ± 0.01	6.35	59.1 ± 6.5
32	S30-3	1.79	3.18	82.1	84.6 ± 0.5	0.07 ± 0.01	5.77	63.1 ± 3.0
33	S36-1	1.17	1.74	22.0	80.0 ± 0.2	0.05 ± 0.01	5.89	–

See Supplement in (Ariskin et al., 2018a) for the composition of the olivine and spinel. Contaminated dunites are printed in semibold type.

the sixteen samples from the Yoko section, LOI values were 0.0 ± 0.5 and 1.1 ± 0.5 wt %. Note that the 2.5 wt % constraint placed on LOI in (Goncharenko et al., 1992) to select the "freshest" samples is equivalent to ~4 wt % with a correction for complete Fe oxidation (Table 2), which corresponds to serpentinized rocks.

Methods. Olivine for studying its oxygen isotope composition was separated from samples in which the composition of olivine has been studied and whose whole-rock composition has been analyzed at the Central Science Laboratory at the University of Tasmania in Hobart, Australia (Ariskin et al., 2018a). Monomineralic olivine fractions (+0.25 to –0.5 mm) were handpicked under a binocular (Zeiss Stemi 2000C) to get rid of aggregates with other minerals and admixtures, washed in acetone to remove dust, and dried. The isotope analysis was carried out with 1 to 1.5 mg of the material.

The oxygen isotope composition was analyzed at the Laboratory for Isotope Geology at the Institute of

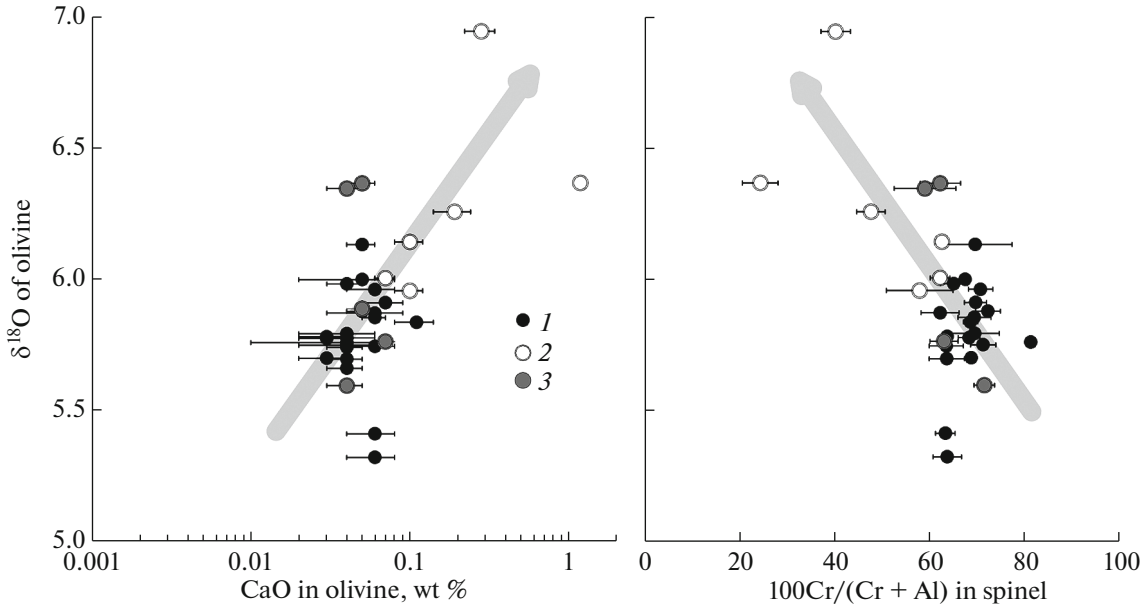

Fig. 2. Correlation between the $\delta^{18}O$ of olivine, CaO concentration of the olivine, and Cr# of spinel in rocks of various type from the Dovyren massif (data from Table 2). Legend: (*1*) uncontaminated rocks from the Yoko and Bolshoi-Tsentralnyi vertical sections; (*2*) contaminated dunites; (*3*) rocks from the Shkolnyi vertical section.

Geology of Ore Deposits, Petrography, Mineralogy and Geochemistry, Russian Academy of Sciences, by means of fluorination with laser heating (Sharp, 1990). In contrast to other methods previously applied to analyze mineral and rock samples from the Dovyren massif, this technique is free of errors related to the incomplete decomposition of the samples (this problem pertains very much to olivine) and those related to measurement standardization. The samples were decomposed with an IR CO_2 laser 30 W in power (New-Wave Research, MIR10-30), with subsequent oxygen extraction with bromine pentafluoride. The mass-spectrometric measurements of the extracted oxygen were made on a DELTAplus (Thermo, Germany) using a dual inlet system. The errors of the measured $\delta^{18}O$ values were no higher than ±0.1‰ (1σ). The measurements were calibrated (on the V-SMOW scale) using two internationally certified standards: UWG-2 garnet and NBS-28 quartz (Spicuzza et al., 1998).

MEASUREMENT AND CALCULATION RESULTS

The measured data on the oxygen isotope composition of the olivine are presented in Table 2, which additionally displays information on the rocks: their normative olivine concentrations, the average composition of olivine in the samples and the Cr# of the coexisting aluminochromite. Olivine from the rocks that do not exhibit any indications of contamination demonstrates $\delta^{18}O$ within a narrow range of 5.8 ± 0.2‰, whereas olivine in the contaminated dunites is slightly enriched in the heavy oxygen isotope (6.2 ± 0.3‰). These are not the highest values ever obtained for olivine from the Dovyren rocks. When the immediate contacts of the magnesian skarns were studied, it was determined that the $\delta^{18}O$ of the olivine may reaches 12–14‰, and that of forsterite in the spinel–forsterite skarns is up to 19‰ (Krivoplyasov et al., 1982). In our situation, the increase in the $\delta^{18}O$ value by ~0.4‰ led us to distinguish a tendency toward olivine enrichment in the ^{18}O isotope where xenoliths of carbonate-replacement skarns occur in the massif, toward their contact zones with the host olivine cumulates. This tendency correlates with mineralogical indications of rock contamination with carbonates (Ariskin et al., 2018a), including elevated CaO concentrations in the olivine and a systematic decrease in the Cr# of the spinel (Fig. 2). In the central part of the Dovyren massif, such contamination effects are discernible within a broad range of depths: from the level of ~500 m to 970 m (Table 1).

It seems to be important that the most homogeneous oxygen isotope composition of the olivine, $\delta^{18}O = 5.8 \pm 0.1$‰, is typical of sixteen freshest rock samples from Mount Yoko. This composition can be assumed as the oxygen isotope composition of olivine that was in equilibrium with the original Dovyren magmas. The $\delta^{18}O$ values of six rocks from the Shkolnyi section is 6.0 ± 0.4‰. The reason for the significant standard deviation in this situation is the contrasting differences between the three samples with $\delta^{18}O$ = 5.6–5.9‰ (which is close to compositions

from the Yoko section) and two samples with 6.4‰ (Table 2). The Cr# of spinel in the latter two samples indicates that the rocks enriched in the ^{18}O isotope are candidates to rocks weakly contaminated with carbonate material, but this is inconsistent with the primary magmatic CaO concentrations of the olivine (Fig. 2). In this instance, it seems to be reasonable to suggest contamination with siliceous terrigenous material: schists or quartzites from the host rocks of the Olokit complex (Rytsk et al., 2002).

Data on the original $\delta^{18}O$ of the olivine can be used to evaluate the local extent of contamination of the primitive magmas and their cumulates with carbonate material when the Dovyren chamber developed and/or in the course of differentiation in this chamber. To do this, it is necessary to proceed from the oxygen isotope composition of the olivine to that of the melt. This can be done for each of the rocks if data are available on the closure temperatures of the cumulus systems in terms of oxygen isotope exchange between the olivine and cumulus melt near the solidus. This problem was solved using modeling results on the equilibrium crystallization of virtual melts whose composition corresponds to the bulk composition of the samples.

Simulation of the equilibrium crystallization of the rocks. The petrological meaning of these calculations is analogous to that of mineralogical thermometry and is underlain by the following three postulates (Ariskin and Barmina, 2004): (1) the bulk composition of a rock sample reflects the composition of a mixture of the cumulus phases and intercumulus liquid; (2) the temperature of the original cumulus mixture corresponds to that of the melt; and (3) the solidification process is associated with systematic changes in the compositions of all phases according to the thermodynamic laws of mineral–melt equilibria. Thus, algorithms for simulating magma crystallization enable one to calculate the trajectory of the compositional evolutions of the melt and equilibrium phases up to complete solidification. The problem is complicated by that the temperature of the original mixture (magma or cumulate) is usually not known, and hence, the complete crystallization trajectory shall be calculated, starting at 100% rock melting (including segments of virtual heterogeneous equilibria) to the solidus. Our situation is simpler: it is important to reach the lowest temperatures, when the last melt portions occur in equilibrium with the whole volume of solids.

The equilibrium crystallization of the rock melts (Table 2) was simulated with the COMAGMAT-5 program package (Ariskin et al., 2018b) in its version 5.2.2.1 (https://comagmat.web.ru/apps-comagmat.html) for normal anhydrous conditions, at a pressure of 1 atm and oxygen fugacity corresponding to QFM – 1 (Ariskin et al., 2017). These parameters are close to the crystallization parameters in the chamber, which were estimated by an independent technique ($P \le 0.5$–1 kbar, water content in the melt <0.5 wt %, oxygen fugacity ≤ QFM) and have already been used in a set of simulations of the parameters of the most primitive Dovyren magmas (Ariskin et al., 2016). This was done using bulk rock compositions from Supplement A in (Ariskin et al., 2018a); the maximum crystallinity was 98%. Figure 3 shows some of the calculated crystallization trajectories. The parameters of the model melts, and the calculated temperatures and olivine and plagioclase compositions near the solidus are reported in Table 3.

The crystallization sequence of sample DV30-2 is shown in Fig. 3 for comparison, because the sample is picrodolerite from the vicinity of the lower contact and is orthocumulate with the most magnesian intercumulus melt, which contained ~11 wt % MgO and ~52 wt % SiO_2 at the temperature of the original magma of 1290°C (Ariskin et al., 2016, 2018a). The evolution of the intercumulus melt during the solidification of the cumulus mixes generating crystallized rocks are calculated at the lowest temperatures, and this pertains to all of the samples.

Except only one sample from the top portion of the Yoko section (07DV229-1), our simulations have demonstrated a broad virtual crystallization field of the olivine (as a result of its accumulation). The samples can be classified into two groups, including "uncontaminated" and "contaminated" rocks. In the former instance, the second phase to crystallize was plagioclase, which was followed by clinopyroxene ± orthopyroxene, i.e., in exact compliance with what was predicted by the crystallization of primitive orthocumulates from the lower contact (Fig. 3). This succession is different from that of the contaminated rocks: the second mineral to crystallize was clinopyroxene (for example, sample 07DV309-1 in Fig. 3). Correspondingly, the near-solidus residual melts evolved in the region of melts strongly undersaturated in silica (<40–30 wt % SiO_2) at temperatures above 1300–1400°C. We regard these estimates as an artifact of the model, although the expansion of the stability field of Ca-pyroxene in systems contaminated with carbonate is far from surprising (Gaeta et al., 2009; Mollo et al., 2010; Di Rosso et al., 2012). This is confirmed by the fact that the rocks contain magnesian diopside (up to diopsidites) and fassaite (Wenzel et al., 2002; Ariskin et al., 2018a). With regard for the uncertainties of the simulations of melt–mineral equilibria in similar systems with the COMAGMAT-5 model, these results were rejected from further considerations. The only exception was sample 07DV309-1, data on which are also placed in Table 3.

For the uncontaminated rocks, the COMAGMAT-5 program package predicts the solidus association *Ol* + *Pl* + *Cpx* ± *Opx,* occasionally with minor sulfide and ilmenite. The temperatures at which crystallization terminated were from 1131 to 1266°C (1176 ± 34°C on average) (Table 3). These variations reflect two factors: (1) the amount of melt buried in the cumulates and (2) the extent of its fractionation in the course of

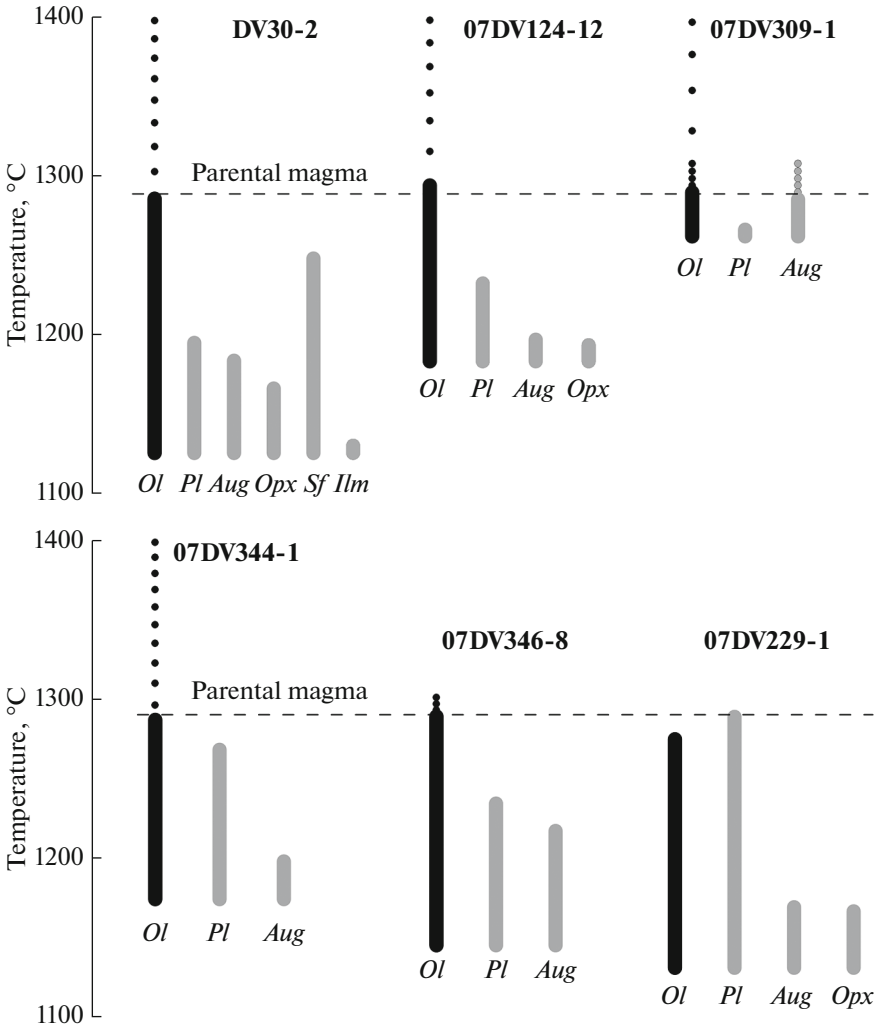

Fig. 3. Simulated crystallization sequences and the lowest temperature mineral associations of the primitive picrodolerite from the lower contact zone of the Dovyren massif (DV30-2) and representative samples in Tables 1 and 2. Simulations with the COMAGMAT-5 program package (Ariskin et al., 2018b) in an approximation of dry systems under atmospheric pressure and QFM – 1 oxygen fugacity. Only results at temperatures below that of the parental magma (1290°C) have a petrological meaning.

solidification of the massif. Correspondingly, the minimum temperature estimates are typical of the porous basal cumulates and rock units near the roof of the massif, which contain the least magnesian olivine and pyroxenes (samples 14–16 in Table 2). The maximum estimates, above 1200°C, are typical of the olivine and troctolite cumulates with the minimum content of intercumulus material.

The plausibility of the modeling results can be estimated based on data in Fig. 4, in which near-liquidus (according to the calculations) and observed (in the rocks provisionally recognized as "uncontaminated") olivine compositions are compared. Although the calculated compositions are obviously shifted to forsterite-poorer compositions, the average deviations are small: 0.96 ± 0.59 mol % *Fo*, and the discrepancies are greater (>2 mol % *Fo*) for a single sample of the uppermost leucotroctolite (sample 07DV229-1, $\Delta = -2.2\%$). A systematic character of this shift may be explained by a slight overestimation of Fe^{2+} in the melt, $Fe^{2+}/\Sigma Fe$ (the simulations were conducted for fairly reducing conditions of QFM – 1) or by the absence of complete equilibrium between the very last melt portions and the crystalline cumulate masses. In any event, these discrepancies do not affect significantly the composition of the model melts, whose temperature variations depending on the redox parameters are commonly do not exceed a few grades (Ariskin and Barmina, 2004). This led us to believe that the parameters of the near-liquidus equilibria of the rocks are predicted reasonably accurately (Table 3).

The **oxygen isotope composition of the parental melt** was calculated based on the approximation (1)

$$\delta^{18}O(Ol) - \delta^{18}O(melt) \approx 1000 \ln \alpha, \quad (1)$$

Table 3. Parameters of model melts, calculated temperatures, the olivine and plagioclase compositions, and the oxygen isotope composition of the residual melts near the solidus of the cumulates

Sample	Sample number	Concentrations (wt %) in the residual melt			Mineral compositions, mol %		T_{98}, °C*	$\delta^{18}O$ in melt, ‰
		SiO_2	Al_2O_3	MgO	*Fo* (*Ol*)	*An* (*Pl*)		
1	07DV340-1	59.2	16.0	4.2	82.1	69.8	1139	6.99
2	07DV232-1	49.1	13.9	7.0	83.5	72.8	1163	6.79
3	07DV231-1	58.9	17.8	3.4	84.2	80.4	1137	6.73
4	07DV341-1	49.7	14.3	8.5	82.2	85.2	1190	6.71
5	07DV341-3	49.3	13.3	7.1	79.1	80.1	1158	6.61
6	07DV343-1	48.8	13.7	7.9	79.8	83.0	1176	6.51
7	07DV344-1	52.3	14.3	7.7	79.9	84.9	1175	6.57
8	07DV223-1	42.7	20.6	8.5	82.1	84.9	1245	6.52
9	07DV224-1	50.7	14.2	8.0	82.9	81.4	1181	6.81
10	07DV226-1	47.8	14.1	8.8	81.7	85.5	1192	6.59
11	07DV346-1	50.6	14.9	8.8	82.9	90.6	1191	6.63
12	07DV346-5	50.4	14.2	8.3	81.1	84.9	1184	6.54
13	07DV346-6	46.0	17.3	8.6	81.5	84.9	1216	6.65
14	07DV346-8	49.5	12.9	6.5	75.7	77.6	1146	6.51
15	07DV228-1	51.4	13.4	6.7	77.2	79.4	1153	6.61
16	07DV229-1	50.7	13.2	6.1	75.4	83.8	1131	6.72
17	07DV124-2	56.2	14.7	6.1	85.0	72.7	1154	6.16
18	07DV124-3	57.3	15.1	6.1	83.9	72.2	1165	6.52
19	07DV124-11	47.7	21.4	7.3	84.9	91.5	1223	6.51
20	07DV124-12	54.4	15.1	7.9	85.7	83.9	1183	6.79
21	07DV124-13	54.4	17.0	6.9	84.9	80.3	1189	6.21
22	07DV124-17	**n.d.**	**n.d.**	**n.d.**	**n.d.**	**n.d.**	**1176****	**6.96**
23	07DV124-20	**n.d.**	**n.d.**	**n.d.**	**n.d.**	**n.d.**	**1176****	**6.82**
24	07DV124-22	**n.d.**	**n.d.**	**n.d.**	**n.d.**	**n.d.**	**1176****	**6.77**
25	07DV309-1	**42.1**	**24.0**	**8.1**	**86.1**	**н.о.**	**1176****	**7.07**
26	07DV131-10	**n.d.**	**n.d.**	**n.d.**	**n.d.**	**n.d.**	**1176****	**7.76**
27	07DV311-1	**n.d.**	**n.d.**	**n.d.**	**n.d.**	**n.d.**	**1176****	**7.18**
28	07DV314-2	45.2	16.7	9.1	82.9	86.6	1217	6.52
29	S08-4	60.9	17.3	3.2	83.2	75.2	1132	7.23
30	S10-7	51.9	15.0	5.9	82.0	79.1	1152	6.43
31	S12-2	60.1	16.6	4.1	85.5	72.7	1145	7.19
32	S30-3	41.8	23.8	7.4	83.6	84.3	1266	6.48
33	S36-1	49.0	13.3	7.2	78.4	81.4	1160	6.72

Calculations with COMAGMAT-5 (Ariskin et al., 2018b). * T_{98} is the temperature at which the crystallinity of the rock is 98%; crystallinity values of 94–96.5% are specified for three samples: 07DV340-1, 311-1, and S12-2. ** Postulated average temperature of all the uncontaminated rocks near the solidus; **n.d.** means not determined.

where α is the isotope fractionation factor between the melt and olivine, which is related to the closure temperature of isotope exchange as

$$1000 \ln \alpha = 10^6 A/T^2, \quad (2)$$

where A is a semiempirical constant, and T is the temperature in K. The calculations were carried out with $A = -1.70$, which was suggested in (Zhao and Zheng, 2003) for volcanic rocks representing systems olivine phenocryst–basaltic glass/lava. Thereby the temperature at which effective isotope exchange ceases to proceed in uncontaminated rocks was assumed as the model temperature in a closed system corresponding to equilibrium between 2% residual melt and 98% crystalline mass (Table 3). For the six contaminated

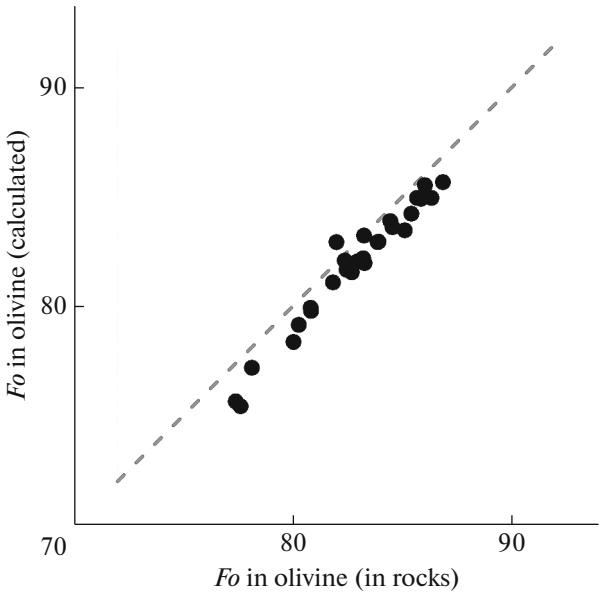

Fig. 4. Correlation between the calculated and observed olivine compositions in uncontaminated rocks of the Dovyren massif (based on data in Tables 2 and 3).

dunites, the temperature of isotope exchange termination was postulated to be the near-liquidus temperature in the closed system, i.e., 1176°C. These assumptions imply that the exchange by oxygen isotopes mostly terminates when the "fluid-melt" is exhausted, and there are no reasons to believe that contaminated melts evolved in another temperature field than that of the host dunites. Note that two-thirds of the samples contained more than 70% olivine (Table 2), which implies that postsolidus reactions (such as olivine–plagioclase) did not any significantly affect the isotope composition of the olivine that crystallized during the late magmatic process.

Table 3 reports the $d^{18}O$ values calculated for all of the samples. According to these data, the average $d^{18}O$ of the intercumulus melts is $6.6 \pm 0.2‰$ of the uncontaminated rocks and $7.1 \pm 0.3‰$ for the rocks with traces of contamination. According to the specified range of the near-solidus temperatures (1131–1266°C), the average isotope shift between the olivine and model melts is $0.81 \pm 0.03‰$.

DISCUSSION

Comparison with data on other layered massifs. Figure 5 compares data on the isotope composition of olivine from the Dovyren massif and other layered intrusions and/or mineralized complexes. According to these data, $\delta^{18}O$ of olivine tends to increase from intrusive bodies related to tholeiitic basalts (mantle sources of MORB type) to mineralized intrusions related to reservoirs with evidence that crustal material was involved in the magma-generating processes and/or evolution of the parental magmas (Wilson, 2012; Maier et al., 2016; Ariskin et al., 2018a; Tang et al., 2018). Our data are the closest to the isotope characteristics of the Paleoproterozoic Bushveld complex, and the average $\delta^{18}O$ values of olivine from the uncontaminated Dovyren rocks practically exactly coincide with the maximum $\delta^{18}O$ values of olivine from the mineralized Jinchuan complex (Ripley et al., 2005). The latter has an age of 831.8 ± 0.6 and was formed, similar to the Dovyren massif, at the breakup of the Rodinia supercontinent (Zhang et al., 2010).

More and more arguments are lately published that intrusive magmatism that produced the mineralized Bushveld and Jinchuan complexes had certain analogous features (Eales and Costin, 2012; Tang et al., 2018). These analogies include two contamination stages of the parental magmas (in the lower and middle crust), which may take place either before the chamber stage or when the magma chamber was formed. The mantle source of the most primitive magmas is uncertain. This source was asthenospheric or metasomatized subcontinental lithospheric mantle (SCLM). The former scenario is discussed with reference to komatiite sills in the bottom part of the Bushveld complex (Wilson, 2012; Maier et al., 2016), and the latter one was suggested for the Jinchuan ultramafic rocks. Isotopic–geochemical data on the Dovyren massif may also suggest such a double-stage scenario for the involvement of crustal material in processes that produced the mantle source and controlled differentiation in the chamber.

The very low $\varepsilon_{Nd}(t)$ values of the Dovyren rocks (-14.8 on average, $t = 728.4$ Ma) cannot be explained by the assimilation of carbonates from the host rocks, which have ε_{Nd} close to -7 (Amelin et al., 1996). This leaves the only possibility of admitting the occurrence of an older mantle protolith with a crustal Sm/Nd ~ 0.22 (Ariskin et al., 2015). Thereby the high Mg# of the original olivine (which was calculated for rocks in the basal zone as $\sim Fo_{88}$) indicates that the Dovyren magmas with crustal signatures possessed a picritoid composition at temperatures of about 1300°C (Ariskin et al., 2018a). These signals of "mantle–crustal" processes correlate with the elevated (relative to the MORB system) $\delta^{18}O$ values of olivine from the uncontaminated rocks (Fig. 5).

At the same time, in addition to the fairly broad variations in the $\delta^{18}O$ of olivine from the uncontaminated rocks, the Dovyren intrusive complex shows evidence of heterogeneities of the Rb–Sr and Sm–Nd systems (Ariskin et al., 2015), which also cannot be explained by the prehistory of the source or by crystallization differentiation alone. This is particularly well seen in the dunite units with xenoliths of carbonate rocks (Wenzel et al., 2002). Despite the long-lasting discussion, the extent of contamination with marble/dolomite and the effects of these processes on differentiation in the Dovyren chamber, i.e., eventually

on the development of the phase layering of the massif, are still largely uncertain.

Estimation of the extent of contamination with carbonate material. Interaction between basaltic magmas and carbonates is commonly described by desilication reactions, including the thermal decomposition of carbonates with the formation of Ca-pyroxene solid solutions (e.g., Mollo et al., 2010):

$$L_1 + \mathrm{CaCO_3} \rightarrow L_2 + Di + CaTs + \mathrm{CO_2}\uparrow, \qquad (3)$$

where L_1 is the uncontaminated melt, *Di* is diopside ($CaMgSi_2O_6$), *CaTs* is pyroxene rich in the Tschermakite component, and L_2 is the newly formed melt depleted in SiO_2 and somewhat enriched in CaO. The parental picritoid magmas of the Dovyren massif contained about 20–30% olivine (Ariskin et al., 2018a), and hence, such reactions should also take into account the presence of cumulus olivine and changes in its composition: an increase in its Mg# and CaO concentration (Wenzel et al., 2002; Di Stefano et al., 2018). This heterogeneity of the reactants and interaction products hampers the successive solution of the oxygen isotope balance with the aim of estimating how much the cumulus associations are contaminated. In a simplified form, this material balance can be described by the equation

$$\delta^{18}\mathrm{O}(L_2) = f\delta^{18}\mathrm{O}(\mathrm{cont.}) + (1-f)\delta^{18}\mathrm{O}(L_1), \qquad (4)$$

where $\delta^{18}O(L_1)$ and $\delta^{18}O(L_2)$ are the oxygen isotope compositions of the uncontaminated and contaminated melts, respectively, δ^{18}O(cont.) characterizes the oxygen isotope composition of the carbonate material, and *f* is the fraction of the contaminant (i.e., the total amount of CaO + MgO + FeO provided by carbonate decomposition for the newly formed silicate phases). Assuming the average $\delta^{18}O$ values for the contaminated (7.1‰) and uncontaminated (6.6‰) melts and $\delta^{18}O$ = 23‰ for the carbonates (Krivoplyasov et al., 1982), we estimated the contribution of the contaminant at ~3.2%. For the heterogeneous cumulus system, the estimated fraction of the contaminant is 0.3–0.4% lower at ~40% olivine crystals and 0.7–1% lower at ~90% crystals.

The aforementioned balance assumes that the oxygen isotope composition of the carbonate decomposition products is either constant or varies insignificantly [see reaction (3)]. In fact, theoretical estimates indicate that oxygen isotope fractionation at temperatures of about 1200°C in the CO_2–$CaCO_3$ system may reach ~2‰ (Chacko and Deines, 2008). This increases the maximum estimated fraction of the contaminant to ~5 and to ~4% at a content of olivine crystals of 90%. Hence, the new melt or cumulus system whose isotope characteristics correspond to equilibrium with olivine from the contaminated dunite zone (Tables 2 and 3) can be obtained by at least 3–5% contamination with dolomite.

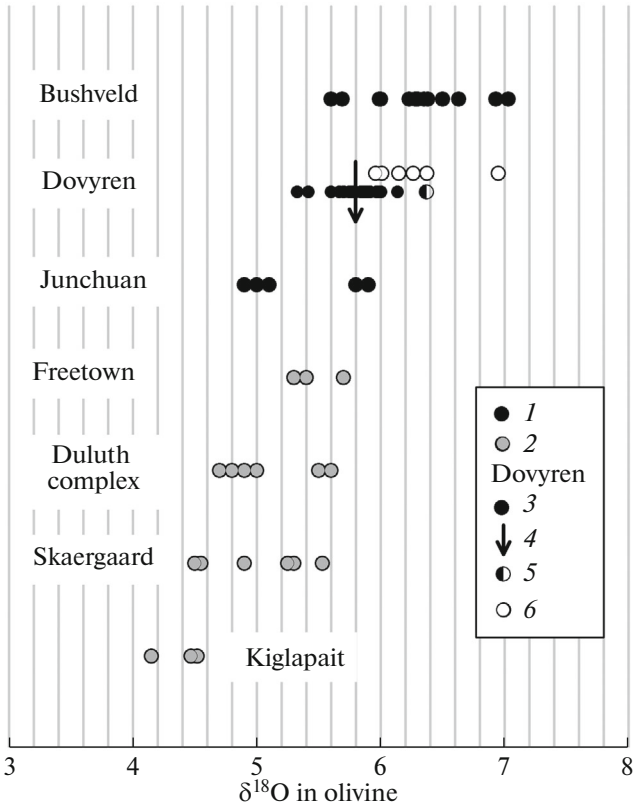

Fig. 5. Oxygen isotope composition of olivine from widely known layered intrusions and mineralized complexes: Bushveld complex (Harris et al., 2005; Gunther et al., 2018); Junchuan (Ripley et al., 2005); Freetown intrusion, Sierra Leone (Chalokwu et al., 1999); South Kawishiwi Intrusion, Duluth complex (Lee and Ripley, 1996); Skaergaard intrusion (Taylor, 1959; Bindeman et al., 2008); and the Kiglapait intrusion (Kalamaradis, 1984). Probable sources: (*1*) likely subcontinental lithospheric mantle (SCLM), (*2*) MORB-type depleted mantle, (*3–6*) Yoko-Dovyren massif: (*3*) uncontaminated rocks, (*4*) average composition of the uncontaminated rocks, (*5*) two "likely contaminated" rocks of the Shkolnyi section, (*6*) contaminated dunites.

Assuming the isotopically heaviest oxygen isotope composition of the contaminated melt (say, $\delta^{18}O$ = 12‰) in equilibrium with olivine from contact zones with the carbonate-replacement skarns ($\delta^{18}O \approx 11$; Krivoplyasov et al., 1982) shall require approximately 30% contaminant. However, such significant contamination is local and is seen as the development of contaminated dunite aureoles around skarnized marble and dolomite relics. This is also evident from the intercumulus composition in these aureoles, in which diopside and fassaite (pyroxene with high alumina concentrations; Wenzel et al., 2002) are the most magnesian, the olivine has higher CaO concentrations and Mg#, and the Al-spinel composition changes (Kislov, 1998; Ariskin et al., 2018a). Reactions between the original magma and carbonates are reflected only in the expansion of the clinopyroxene stability field, as was

determined by simulation the equilibrium crystallization of contaminated rocks with the COMAGMAT-5 program package.

CONCLUSIONS

(1) Fluorination with laser heating was applied to study the oxygen isotope composition of olivine in plagiolherzolites, dunites, troctolites, and olivine gabbronorites of the Yoko-Dovyren layered massif. Most of the $\delta^{18}O$ values of olivine from the freshest and uncontaminated rocks ($n = 27$) lie within the range of $5.8 \pm 0.2‰$. The weakly and strongly contaminated dunites show a notably heavier oxygen isotope composition: up to $6.2 \pm 0.3‰$. Such compositions are demonstrated to be the closest to those in other mineralized complexes such as Bushveld and Jinchuan.

(2) The COMAGMAT-5 software (Ariskin et al., 2018b) was applied to simulate the crystallization trajectories of the cumulus rocks, including the equilibrium phase proportions at temperatures corresponding to 2% residual melt. These near-solidus temperatures span the range of 1131–1266°C (1176 ± 34°C on average) and are viewed as the temperatures at which the cumulus systems became closed with respect to oxygen isotope exchange between the olivine and melt after the intercumulus melt as mobile "fluid" has been exhausted.

(3) Data on the oxygen isotope composition of the olivine and model temperatures of the closure of this mineral, as well as $\delta^{18}O$ are calculated for each of the rocks for melts in equilibrium with the olivine. The average $\delta^{18}O$ value was $6.6 \pm 0.2‰$ for the intercumulus melts of the uncontaminated rocks, and $7.1 \pm 0.2‰$ for the melts with traces of contamination with crustal material.

(4) According to estimates with the balance model for melt contamination with dolomite, the main dunite volume in the core of the massif was no more than 3–5 wt % contaminated. The isotope characteristics of melts in aureoles near contacts with xenoliths of carbonate-replacement skarns indicate that these melts may have dissolved up to 30% carbonates.

ACKNOWLEDGMENTS

The authors thank V.B. Polyakov (Institute of Experimental Mineralogy, Russian Academy of Sciences) for valuable comments on the manuscript and O.A. Lukanin (Vernadsky Institute of Geochemistry and Analytical Chemistry, Russian Academy of Sciences).

FUNDING

This study was supported by the Russian Science Foundation, project no. 16-17-10129. The oxygen isotope composition of olivine was studied under government-financed research project 0136-2019-0013 for the Institute of Geology of Ore Deposits, Petrography, Mineralogy and Geochemistry (IGEM), Russian Academy of Sciences. Olivine samples for this research were prepared under government-financed research project for the Vernadsky Institute of Geochemistry and Analytical Chemistry (GEOKhI), Russian Academy of Sciences.

REFERENCES

Yu. V. Amelin, L. A. Neymark, E. Yu. Ritsk, and A. A. Nemchin, "Enriched Nd–Sr–Pb isotopic signatures in the Dovyren layered intrusion (eastern Siberia, Russia): evidence for contamination by ancient upper–crustal material," Chem. Geol. **129**, 39–69 (1996).

A. A. Ariskin and G. S. Barmina, "COMAGMAT: development of a magma crystallization model and its petrologic applications," Geochem. Int. **42**, S1–S157 (2004).

A. A. Ariskin, Yu. A. Kostitsyn, E. G. Konnikov, L. V. Danyushevsky, S. Meffre, G. S. Nikolaev, A. McNeill, E. V. Kislov, and D. A. Orsoev, "Geochronology of the Dovyren intrusive complex, Northwestern Baikal area, Russia, in the Neoproterozoic," Geochem. Int. **51** (11), 859–875 (2013).

A. A. Ariskin, L. V. Danyushevsky, E. G. Konnikov, R. Maas, Yu. A. Kostitsyn, E. McNeill, S. Meffre, G. S. Nikolaev, and E. V. Kislov, "The Dovyren intrusive coplex (northern Baikal region, Russia): isotope–geochemical markers of contamination of parental magmas and extreme enrichment of the source," Russ. Geol. Geophys. **56** (3), 411–434 (2015).

A. A. Ariskin, E. V. Kislov, L. V. Danyushevsky, G. S. Nikolaev, M. L. Fiorentini, S. Gilbert, K. Goemann, and A. Malyshev, "Cu–Ni–PGE fertility of the Yoko–Dovyren layered massif (Northern Transbaikalia, Russia): thermodynamic modeling of sulfide compositions in low mineralized dunite based on quantitative sulfide mineralogy," Mineral. Deposita **51**, 993–1011 (2016).

A. A. Ariskin, I. S. Fomin, E. V. Zharkova, A. A. Kadik, and G. S. Nikolaev, "Redox conditions during crystallization of ultramafic and gabbroic rocks of the Yoko–Dovyren Massif (based on the results of measurements of intrinsic oxygen fugacity of olivine)," Geochem. Int. **55** (7), 595–607 (2017).

A. A. Ariskin, K. A. Bychkov, G. S. Nikolaev, and G. S. Barmina, "The COMAGMAT-5: Modeling the effect of Fe–Ni sulfide immiscibility in crystallizing magmas and cumulates," J. Petrol. **59**, 283–298 (2018).

A. Ariskin, L. G. Danyushevsky, Nikolaev, E. Kislov, M. Fiorentini, A. McNeill, Yu. Kostitsyn, K. Goemann, S. Feig, and A. Malyshev, "The Dovyren Intrusive Complex (Southern Siberia, Russia): Insights into dynamics of an open magma chamber with implications for parental magma origin, composition, and Cu–Ni–PGE fertility," Lithos **302**, 242–262 (2018).

A. A. Ariskin, L. V. Danyushevsky, M. Fiorentinin, G. S. Nikolaev, E. V. Kislov, I. V. Pshenitsyn, V. O. Yapaskurt, and S. N. Sobolev, "Petrology, geochemistry, and origin of sulfide–bearing and PGE–mineralized troctolites from the Konnikov zone in the Yoko–Dovyren layered intrusion," Russ. Geol. Geophys. **62** (5–6), 611–633 (2020).

V. P. Bushuev and R. S. Tarasov, The Kholodninskoe Sulfide–Base Metal Deposit. Report of the Kholodninskaya GRP for 1975–84 (Buryatgeologiya, Ulan–Ude, 1984) [in Russian].

T. Chacko and P. Deines, "Theoretical calculation of oxygen isotope fractionation factors in carbonate systems," Geochim. Cosmochim. Acta. **72**, 3642–3660 (2008).

C. I. Chalokwu, E. M. Ripley, and Y.-R. Park "Oxygen isotopic systematics of an open–system magma chamber: An example from the Freetown Layered Complex of Sierra Leone," Geochim. Cosmochim. Acta **63** (5), 675–685 (1999).

R. N. Clayton and T. K. Mayeda, "The use of bromine pentafluoride in the extraction of oxygen from oxides and silicates for isotopic analysis," Geochim. Cosmochim. Acta **27**, 43–52 (1963).

T. Di Rocco, C. Freda, M. Gaeta, S. Mollo, and L. Dallai "Magma chambers emplaced in carbonate substrate: petrogenesis of skarn and cumulate rocks and implications for CO_2 degassing in volcanic areas," J. Petrol. **53**, 2307–2332 (2012).

F. Di Stefano, S. Mollo, P. Scarlato, M. Nazzari, O. Bachmann, and M. Caruso, "Olivine compositional changes in primitive magmatic skarn environments: A reassessment of divalent cation partitioning models to quantify the effect of carbonate assimilation," Lithos. **316–317**, 104–121 (2018).

V. V. Distler and A. G. Stepin, "Low-sulfide PGE–bearing horizon of the Yoko–Dovyren layered ultramafic–mafic intrusion, Northern Baikal area," Dokl. Akad. Nauk **328** (4), 498–501 (1993).

H. W. Eales and G. Costin "Crustally contaminated komatiite: primary source of the chromitites and Marginal, Lower, and Critical Zone magmas in a staging chamber beneath the Bushveld Complex," Econ. Geol. **107**, 645–665 (2012).

R. E. Ernst, M. A. Hamilton, U. Söderlund, J. A. Hanes, D. P. Gladkochub, A. V. Okrugin, T. Kolotilina, A. S. Mekhonoshin, W. Bleeker, A. N. LeCheminant, K. L. Buchan, K. R. Chamberlain, and A. N. Didenko, "Long-lived connection between southern Siberia and northern Laurentia in the Proterozoic," Nature Geosci. **9**, 464–469 (2016).

M. Gaeta, T. Di Rocco, and C. Freda, "Carbonate assimilation in open magmatic systems; the role of melt–bearing skarns and cumulate-forming processes," J. Petrol. **50**, 361–385 (2009).

A. I. Goncharenko, I. F. Gertner, and Yu. A. Fomin, "Evolution of oxygen isotope composition in olivines from the Yoko–Dovyren Pluton," Geol. Geofiz. **12**, 63–71 (1992).

T. Günther, K. M. Haase, M. Junge, T. Oberthür, D. Woelki, and S. Krumm, "Oxygen isotope and trace element compositions of platiniferous dunite pipes of the Bushveld Complex, South Africa – signals from a recycled mantle component?" Lithos. **310–311**, 332–341 (2018).

S. A. Gurulev, *Geology and Conditions of Formation of the Yoko–Dovyren Gabbro–Peridotite Massif* (Nauka, Moscow, 1965) [in Russian].

C. Harris, J. J. M. Pronost, L. Ashwal, and R. G. Cawthorn, "Oxygen and hydrogen isotope stratigraphy of the Rustenburg Layered Suite, Bushveld Complex: constraints on crustal contamination," J. Petrol. **46**, 579–601 (2005).

E. Ito, W. M. White, and C. Gopel, "The O, Sr, and Pb isotope geochemistry of MORB," Chem. Geol. **62**, 157–176 (1987).

R. I. Kalamarides, "Kiglapait geochemistry VI: oxygen isotopes," Geochim. Cosmochim. Acta **48**, 1827–1836 (1984).

E. V. Kislov, *Yoko–Dovyren Layered Massif* (BNTs SO RAN, Ulan-Ude, 1998) [in Russian].

E. G. Konnikov, *Precambrian Differentiated Ultramafic–Mafic Complexes of Transbaikalia* (Nauka, Novosibirsk, 1986) [in Russian].

E. G. Konnikov, W. P. Meurer, S. S. Neruchev, E. M. Prasolov, E. V. Kislov, and D. A. Orsoev, "Fluid regime of platinum group elements (PGE) and gold-bearing reef formation in the Dovyren mafic–ultramafuc layered complex, eastern Siberia, Russia," Mineral. Deposita **35**, 526–532 (2000).

G. S. Krivoplyasov, A. A. Yaroshevsky, V. I. Ustinov, and V. P. Strizhov, "Redistribution of oxygen isotopes during interaction of magmatic systems with host rocks: evidence from the Yoko–Dovyren layered massif, northern Baikal area," *Proc. 9th All–Union Symposium on Stable Isotopes in Geochemistry* (GEOKHI AN SSSR, Moscow, 1982), pp. 134–136.

G. S. Krivoplyasov, A. A. Yaroshevsky, and V. I. Ustinov, "Oxygen isotope composition of rock–forming minerals of some differentiated trap sills and large layered intrusion: evidence from traps of the Norilsk district, Podkamennaya Tunguska River, and Yoko–Dovyren massif)," *Proc. 10th All–Union Symposium on Stable Isotopes in Geochemistry, Moscow, Russia, 1984* (GEOKHI RAS, Moscow, 1984), p. 233 [in Russian].

P. J. Lechler and M. O. Desilets, "A review of the use of loss on ignition as a measurement of total volatiles in whole–rock analysis, Chem. Geol. **63**, 341–344 (1987).

I. Lee and E. M. Ripley, "Mineralogic and oxygen isotopic studies of open system magmatic processes in the South Kawishiwi Intrusion, Spruce Road area, Duluth Complex, Minnesota," J. Petrol. **37**, 1437–1461 (1996).

W. D. Maier, S.-J. Barnes, and B. T. Karykowski A chilled margin of komatiite and Mg–rich basaltic andesite in the western Bushveld Complex, South Africa. Contrib. Mineral. Petrol. **171**, 1–22 (2016).

S. Mollo, M. Gaeta, C. Freda, T. Di Rocco, V. Misiti, and P. Scarlato, "Carbonate assimilation in magmas: A reappraisal based on experimental petrology," Lithos **114**, 503–514 (2010).

D. A. Orsoev, "Distribution of oxygen isotopes in rocks and minerals from the Critical Zone of the Ioko–Dovyren Pluton," Geol. Ore Deposits **52**, 543–550 (2010).

D. A. Orsoev, "Anorthosites of the low–sulfide platiniferous horizon (Reef I) in the Upper Riphean Yoko–Dovyren Massif (Northern Cisbaikalia): new data on the composition, PGE–Cu–Ni Mineralization, fluid regime, and formation conditions," Geol. Ore Deposits **61** (4), 306–332 (2019).

D. A. Orsoev, E. V. Kislov, E. G. Konnikov, S. V. Kanakin, and A. B. Kulikova, "Distribution and compositional features of PGE–bearing horizons of the Yoko–

Dovyren latered massif, Northern Baikal area," Dokl. Akad. Nauk **340** (2), 225–228 (1995).

N. N. Pertsev, and L. I. Shabyllin, "Skarn, carbonate, and brucite xenoliths of the Yoko-Dovyren massif," *Contact Processes and Mineralization in the Gabbro–Peridotite Intrusions* (Nauka, Moscow, 1979), pp. 85–96 [in Russian]

N. N. Pertsev, E. G. Konnikov, E. V. Kislov, D. A. Orsoev, and A. N. Nekrasov, "Merwinite–Facies magnesian skarns in xenoliths from dunite of the Dovyren layered intrusion," Petrology **11** (5), 464–475 (2003).

G. V. Polyakov, N. D. Tolstykh, A. S. Mekhonoshin, A. E. Izokh, M. Yu. Podlipskii, D. A. Orsoev, and T. B. Kolotilina, "Ultramafic–mafic igneous complexes of the Precambrian East Siberian metallogenic province (southern framing of the Siberian craton): age, composition, origin, and ore potential," Russ. Geol. Geophys. **54** (11), 1319–1331 (2013).

E. M. Ripley, A. Sarkar, and C. Li, "Mineralogic and stable isotope studies of hydrothermal alteration at the Jinchuan Ni–Cu deposit, China," Econ. Geol. **100**, 1349–1361 (2005).

E. Yu. Rytsk, V. S. Shalaev, N. G. Rizvanova, R. Sh. Krymskii, A. F. Makeev, and G. V. Rile, "The Olokit Zone of the Baikal fold region: new isotope-geochronological and petrogeochemical data," Geotectonics **36** (1), 24–35 (2002).

Z. D. Sharp, "A laser-based microanalytical method for the in-situ determination of oxygen isotope ratios of silicates and oxides," Geochim. Cosmochim. Acta **54**, 1353–1357 (1990).

M. J. Spicuzza, J. W. Valley, M. J. Kohn, J. P. Girard, and A. M. Fouillac, "The rapid heating, defocused beam technique: a CO_2–laser-based method for highly precise and accurate determination of $\delta^{18}O$ values of quartz," Chem. Geol. **144**, 195–203 (1998).

E. M. Spiridonov, "Barium minerals barite and chlorine dominant ferrokinoshitalite $BaFe_3^{2+}[Cl_2/Al_2Si_2O_{10}]$ in plagioperidotites of the Yoko-Dovyren intrusion, northern Baikal Area: products of epigenetic low–grade metamorphism," Geochem. Int. **57** (11), 1221–1229 (2019).

A. G. Stepin and A. I. Vlasenko, Results of Prospecting Works within the Yoko–Dovyren and Bezymyanny Mafic–Ultramafic Massifs. Report of the Dovyren Team for 1989–1993 (Buryatgeolkom, Nizhneangarsk, 1994) [in Russian].

Q. Tang, J. Jian Bao, Y. Dang, S. Ke, and Y. Zhao, "Mg–Sr–Nd isotopic constraints on the genesis of the giant Jinchuan Ni–Cu–(PGE) sulfide deposit, NW China," Earth Planet. Sci. Let. **502**, 221–230 (2018).

H. P. Taylor and S. Epstein, "Relation between $^{18}O/^{16}O$ ratios in coexisting minerals of igneous and metamorphic rocks. I Principles and experimental results," Geol. Soc. Am. Bull. **73**, 461–480 (1962).

H. P. Taylor, Jr. and S. Epstein, "O^{18}/O^{16} ratios in rocks and coexisting minerals of the Skaergaard intrusion," J. Petrol. **4**, 51–74 (1963).

S. R. Taylor and S. M. McLennan, *The Continental Crust: its Composition and Evolution* (Blackwell Sci. Pub., Oxford, 1985).

V. I. Ustinov, A. A. Yaroshevksy, V. P. Striglov, and V. F. Sukhverkhov, "Oxygen isotope composition of rock–forming minerals of the Yoko-Dovyren dunite–troctolite–gabbronorite massif, Northern Baikal area," *Proc. 8th All–Union Symposium on Stable Isotopes in Geochemistry* (Moscow, 1980), pp. 56––58.

T. Wenzel, L. P. Baumgartner, G. E. Bruegman, E. G. Konnikov, and E. V. Kislov, "Partial melting and assimilation of dolomitic xenoliths by mafic magma: the Ioko–Dovyren intrusion (North Baikal Region, Russia)," J. Petrol. **43**, 2049–2074 (2002).

A. H. Wilson, "A chill sequence to the Bushveld Complex: insight into the first stage of emplacement and implications for the parental magmas," J. Petrol. **53**, 1123–1168 (2012).

M. Zhang, S. L. Kamo, C. Li, P. Hu, and E. M. Ripley, "Precise U–Pb zirconbaddeleyite age of the Jinchuan sulfide ore-bearing ultramafic intrusion, western China," Mineral. Deposita. **45**, 3–9 (2010).

Z. F. Zhao and Y. F. Zheng, "Calculation of oxygen isotope fractionation in magmatic rocks," Chem. Geol. **193**, 59–80 (2003).

Translated by E. Kurdyukov